# Dielectric Measurement of Individual Microtubules Using the Electroorientation Method

Itsushi Minoura and Etsuko Muto
Brain Developmental Research Group, RIKEN Brain Science Institute, Wako, Japan

ABSTRACT Little is known about the electrostatic/dynamic properties of microtubules, which are considered to underlie their electrostatic interactions with various proteins such as motor proteins, microtubule-associated proteins, and microtubules themselves (lateral association of microtubules). To measure the dielectric properties of microtubules, we developed an experiment system in which the electroorientation of microtubules was observed under a dark-field microscope. Upon application of an alternating electric field (0.5–1.9 $\times$ $10^5$ V/m, 10 kHz–3 MHz), the microtubules were oriented parallel to the field line in a few seconds because of the dipole moment induced along their long axes. The process of this orientation was analyzed based on a dielectric ellipsoid model, and the conductivity and dielectric constant of each microtubule were calculated. The analyses revealed that the microtubules were highly conductive, which is consistent with the counterion polarization model—counterions bound to highly negatively charged microtubules can move along the long axis, and this mobility might be the origin of the high conductivity. Our experiment system provides a useful tool to quantitatively evaluate the polyelectrolyte nature of microtubules, thus paving the way for future studies aiming to understand the physicochemical mechanism underlying the electrostatic interactions of microtubules with various proteins.

## INTRODUCTION

Microtubules of eukaryotic cells play an important role in cellular organization, intracellular transport, and cell motility. In these cellular processes, microtubules serve as molecular tracks for motor proteins such as kinesin and dynein (1) and interact with a variety of microtubule-associated proteins (MAPs) (2).

Electrostatic interaction is thought to play an essential role in mediating these intermolecular interactions of the microtubules. For instance, the processive movement of the motor protein kinesin is modulated by its electrostatic interaction with the microtubule; the distance traveled by the kinesin along the microtubule is dramatically reduced by treatment with high salt concentration or by proteolytic removal of the acidic C-terminal tails of tubulin (3,4). This indicates that this part of the microtubule may serve as an electrostatic tether that keeps the kinesin molecule close to the microtubule surface. A similar decrease was observed in the distance traveled by cytoplasmic dynein by the proteolytic removal of the C-terminal region of tubulin (5). The electrostatic interaction is also implicated in the lateral association of microtubules, which leads to the formation of a variety of cellular architectures composed of microtubule bundles. In this context, the ability of microtubules to form bundles is affected by the presence of ions (6) or MAPs (7,8) in solution. The morphology of the bundle appears to depend on the species of ions (9) or the number of charges included in the microtubule-binding domain of the MAPs (10). These results indicate that both ions and MAPs may serve as cationic ligands that neutralize the negative charges of microtubules (9,10), although the formulation for these observations in terms of electrostatic interaction has not yet been presented.

Despite the potential significance of electrostatic interactions in mediating and regulating their intermolecular interactions, little is known about the electrostatic/dynamic properties of microtubules (11,12). This situation contrasts with the case of other biomolecular filaments such as DNA and actin; the polyelectrolyte nature of these polymers has been extensively characterized, and theoretical studies to explain the observed phenomena are underway (13–19).

To characterize the electrostatic/dynamic properties of microtubules, we performed dielectric measurements by using the electroorientation method (20,21). An alternating electric field was applied to microtubules, inducing dipoles and aligning them parallel to the direction of the applied field. By analysis of this electroorientation process, the microtubule conductivity was calculated to be 1.5 $\pm$ 0.1 mS/m, which is $>$15 times that of the surrounding medium. This high conductivity is probably due to counterion polarization (22–24). Since the microtubule has a large negative potential (12), counterions bind loosely and nonspecifically to it, whereas their diffusional motion along the long axis is unconstrained. Thus, the high conductivity is mainly attributed to the longitudinal movement of these counterions in response to the applied field. The polyelectrolyte nature of microtubules characterized in this study might define the physicochemical basis for nonspecific electrostatic interactions between microtubules and various proteins.

*Submitted July 25, 2005, and accepted for publication February 7, 2006.*

Address reprint requests to Etsuko Muto, Brain Developmental Research Group, RIKEN Brain Science Institute, 2-1 Hirosawa, Wako 351-0198, Japan. E-mail: emuto@brain.riken.jp.



0006-3495/06/05/3739/10 $2.00

doi: 10.1529/biophysj.105.071324

## MATERIALS AND METHODS

### Preparation of proteins

Tubulin was prepared from porcine brain by temperature-dependent cycles of polymerization and depolymerization (25). Tubulin depleted of MAPs was obtained by performing the second cycle of polymerization in a buffer containing 0.5 M piperazine-1,4-bis(2-ethanesulfonic acid) (PIPES) (pH 6.8) and 10% dimethylsulfoxide (DMSO) (26). Microtubules with lengths of 3–20 $\mu$m were polymerized using a short polymer segment as a seed for polymerization (27) in BRB80 buffer (80 mM 2-morpholinoethanesulfonic acid (MES) (pH 6.8), 2 mM $MgCl_2$, and 1 mM EGTA). The polymerized microtubules were stabilized by 0.2 mM taxol (T7402, Sigma, St. Louis, MO) and centrifuged at 250,000 $\times$ $g$ for 12 min through glycerol cushions (40% v/v glycerol in the BRB80 buffer). The resulting pellet was resuspended in the BRB80 buffer containing 0.2 mM taxol at a final protein concentration of 15 mg/ml; it was stored on ice until use.

For the preparation of subtilisin-treated microtubules (s-MTs), taxol-stabilized microtubules in the BRB80 buffer (3 mg/ml) were incubated with subtilisin (P-5380, Sigma) at a molar ratio of 1:1 (tubulin dimer/subtilisin) at 37°C for 2 h (28). The reaction was stopped by 2 mM phenylmethylsulfonyl fluoride, and the mixture was centrifuged through a glycerol cushion to separate the microtubules from the enzyme and C-terminal fragments. The pellet was then resuspended in the BRB80 buffer containing 0.2 mM taxol. The digestion of both $\alpha$- and $\beta$-tubulin was confirmed by SDS polyacrylamide gel electrophoresis.

To determine the site of subtilisin cleavage, amino acid sequencing with liquid chromatography/mass spectrometry (LC/MS; LCQ-DEACA XP, ThermoQuest, San Jose, CA) was carried out on subtilisin-treated tubulin. LC/MS analysis of the subtilisin-treated $\alpha$-tubulin detected two cleavage sites—at positions $Asp^{438}$ and $Glu^{443}$. The cleavage site in $\beta$-tubulin was not uniquely determined because of its multiple isoforms; the possible cleavage site is at position $Ala^{430}$, $Asp^{431}$, $Glu^{432}$, $Gln^{433}$, or $Gly^{434}$.

### Buffer condition

A low-salt buffer (LS buffer) composed of 1 mM MES (pH 6.7), 10 $\mu$M $MgCl_2$, and 80 $\mu$M EGTA, supplemented with 10 $\mu$M taxol in DMSO, was used for electroorientation. The final concentration of DMSO was 1%. The LS buffer had a free $Mg^{2+}$ concentration of 9.95 $\mu$M, as calculated by the method of Goldstein (29). The conductivity of this buffer solution was 9.7 mS/m, as measured with a conductivity meter (Horiba, Kyoto, Japan). The microtubules were stable in this solution for at least 3 h; all experiments were completed within 1 h of the microtubules being transferred to the LS buffer. EGTA was excluded from the LS buffer in electroorientation experiments for testing the effect of ion species.

### Application of electric fields and observation of electroorientation

The orientation chamber with dimensions 6 mm $\times$ 6 mm $\times$ 0.15 mm was composed of a glass slide and a coverslip that were affixed to each other by means of double-sticky tape (Fig. 1 *A*). A pair of transparent electrodes was microfabricated on the upper surface of the glass slide; a 1500-Å-thick indium-tin-oxide (ITO)-precoated glass surface (Sanyo Shinku, Osaka, Japan) was etched by photolithography to form a pair of parallel electrodes with a spacing of 100 $\pm$ 1 $\mu$m. Each of these ITO electrodes was connected to a coaxial cable by means of a flexible phosphor bronze plate.

For the orientation experiment, a 7-$\mu$l microtubule solution, diluted to a final concentration of $\sim$1 $\mu$g/ml with the LS buffer, was first applied in the open orientation chamber; a coverslip was then placed on the top of the chamber to complete the ceiling. The motion of individual microtubules was observed under a dark-field microscope (Olympus, Tokyo, Japan) with a 50×, 0.5–0.9 NA oil-immersion objective lens (Olympus) and 100 W mercury-lamp illumination (OSRAM, Munich, Germany). Dark-field images were projected onto an electron-bombarded charge-coupled device camera (C7190 Hamamatsu Photonics, Hamamatsu, Japan) and stored using a videocassette recorder.

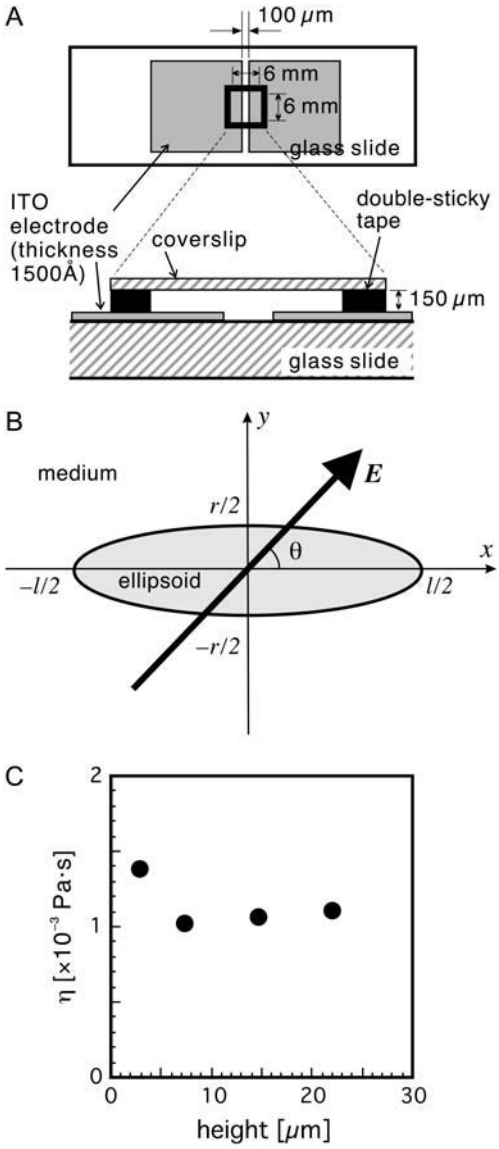


FIGURE 1 (*A*) Top and side views of the electroorientation chamber. Side view is vertically expanded to emphasize the structure. (*B*) Diagram illustrating a dielectric ellipsoid with its long axis $x$ placed at angle $\theta$ to the external field $E$. The $z$ axis is perpendicular to the page. (*C*) Viscosity in the chamber is plotted as a function of the distance from the bottom of the electroorientation chamber. The rotational diffusion constant of microtubule $D_r$ was measured from the mean square rotation angle of the microtubule $\langle\theta^2\rangle$, and $\eta$ was calculated from $D_r = kT/\pi\eta l^3 C_r = \langle\theta^2\rangle/2t$, where $C_r$ is a form factor (Eq. 5) (55).

To apply the AC field to the microtubule solution, sinusoidal voltage in the frequency range of 1 kHz–10 MHz was generated by a function generator (WAVE Factory 1952, NF Co., Yokohama, Japan) and amplified up to 22 V rms (at 1 MHz) by a power amplifier (High Speed Power Amplifier 4055, NF Co.). The applied sinusoidal voltage was monitored using a digital oscilloscope.

The voltage applied to the electrode may get damped due to the resistance, capacitance, and polarization of the electrodes. Therefore, the voltage actually applied in the microtubule solution was estimated by the method of

Schwan (30), i.e., by using an electronic circuit simulation program (Circuit Maker, Altium, Sydney, Australia). In this simulation, the electrode resistance (1 Ω) was taken into account and coaxial cables were modeled as ideal transmission lines. The capacitance and resistance between the electrodes were measured using an impedance meter (Hioki E. E. Co., Ueda, Japan). The voltage drop caused by the impedance of the electrodes was thus estimated to be <1% at frequencies >10 kHz. The voltage drop increased at frequencies <10 kHz, and was estimated to be 6% at 1 kHz.

As the electric field was not uniformly generated near the edge of the ITO electrodes, dielectrophoresis of the microtubules was inevitable in that area (20). Thus, to avoid the effect of dielectrophoresis, the electroorientation of only the microtubules located in the central region of the chamber (>30 $\mu$m from the edges of both the electrodes) was analyzed. Experiments were performed at 25 ± 0.5°C.

## Electroorientation model and calculation of microtubule polarization

Since the orientation is caused by an electric-field-induced torque acting on a microtubule filament, the orientation process was modeled as described below, following the equivalent dipole moment method (31,32).

The microtubule is considered as an ellipsoid with rotational symmetry of length $l$ and radius $r$ (Fig. 1 *B*). When the ellipsoid is placed with its long axis at angle $\theta$ to the electric field $\mathbf{E}^*$, the electrostatic torque exerted on the ellipsoid is calculated by

$$\mathbf{T}_e = 1/2\mathrm{Re}[\mathbf{p}^* \times \mathbf{E}^*], \tag{1}$$

where $\mathbf{p}^*$ is the dipole moment induced in the ellipsoid and Re[ ] denotes the real part. If we take the coordinate $x$ in the direction of the longest axis of the ellipsoid and coordinate $y$ perpendicular to it (both $x$ and $y$ are in the plane parallel to the direction of applied electric field), the orientation of the ellipsoid is caused by the torque about the $z$ axis, which is perpendicular to the direction of electric field. This torque is thus expressed as

$$T_{ez} = 1/2\alpha E^2 \cos\theta \sin\theta, \tag{2}$$

where

$$\alpha = \mathrm{Re}[a_x^* - a_y^*] \tag{3}$$

is the effective polarization coefficient of the ellipsoid, $E = |\mathbf{E}^*|$, and $a_x^*$ and $a_y^*$ are the polarizability of the ellipsoid in the $x$ and $y$ directions, respectively.

On the other hand, the viscous countertorque $T_v$ experienced by the ellipsoid is given by

$$T_v = \pi l^3 \eta C_r \frac{d\theta}{dt}, \tag{4}$$

where $\eta = 1.0 \times 10^{-3}$ Pa·s (see Fig. 1 *C*) is the viscosity of the medium, and $C_r$ is a form factor. Assuming that $l \gg r$, $C_r$ can be expressed as

$$C_r = \frac{1}{3(\ln(l/r) - 1/2)}, \tag{5}$$

where $r$ is 12.5 nm for the microtubule.

The electrostatic torque should be balanced with the viscous countertorque by equating Eqs. 2 and 4, thus resulting in the following equation of motion:

$$\tau \frac{d\theta}{dt} = -\cos\theta \sin\theta, \tag{6}$$

where $\tau$ is the time constant of the orientation expressed as

$$\tau = \frac{2\pi l^2 \eta C_r}{(\alpha/l) E^2}. \tag{7}$$

Eq. 6 can be solved analytically for the case in which the field is applied stepwise with the initial condition $\theta = \theta_0$ at $t = 0$. The solution is

$$\ln(\tan\theta) = \ln(\tan\theta_0) - t/\tau. \tag{8}$$

Based on these equations, the time constant of the orientation, $\tau$, was calculated from the orientation angle of the ellipsoid measured as a function of time (Eq. 8), and the effective polarization coefficient of the microtubule, $\alpha$, was obtained (Eq. 7).

## Calculation of microtubule conductivity

The effective polarization coefficient $\alpha = \mathrm{Re}[a_x^* - a_y^*]$ is actually a parameter related to both the conductivity and dielectric constant of an ellipsoid. For a high aspect ratio ellipsoid such as a microtubule, $a_x^*$ and $a_y^*$ can be approximated by the following equations (32,33):

$$\begin{aligned} \alpha_x^* &= \varepsilon_0 \varepsilon_1 V(\varepsilon_2^* - \varepsilon_1^*)/\varepsilon_1^* \\ \alpha_y^* &= \varepsilon_0 \varepsilon_1 V(\varepsilon_2^* - \varepsilon_1^*)/(\varepsilon_2^* + \varepsilon_1^*), \end{aligned} \tag{9}$$

where

$$\varepsilon_j^* = \varepsilon_j - i\sigma_j/2\pi f \varepsilon_0. \tag{10}$$

$\varepsilon_j^*$ is the complex dielectric constant ($j = 1$ for the surrounding medium and 2 for the microtubule), $\varepsilon_j$ is the dielectric constant, $\sigma_j$ is the conductivity, $\varepsilon_0$ is the permittivity of free space, $V$ is the volume of the ellipsoid, and $f$ is the frequency of the applied field. The dielectric constant of water at 25°C, $\varepsilon_1$, is 78.5. According to these equations, $\sigma_2$ and $\varepsilon_2$ can be obtained by fitting the spectrum of $\alpha/l$.

In the actual experiment, since the electroorientation was performed in a solution with low ionic strength, a cloud of counterions surrounding the microtubule may have significantly affected the orientation. Therefore, to calculate the conductivity, the entire microtubule including the surrounding counterion cloud was regarded as a polar entity of an ellipsoid, the radius of which was represented by the sum of the radius of the microtubule (12.5 nm) and the Debye length in the LS buffer ($\kappa^{-1} = (\sum_i \rho_i e^2 z_i^2/\varepsilon\varepsilon_0 kT)^{-1/2} = 9.1$ nm (34), where $\rho_i$ is the concentration of ions in $m^{-3}$, $z_i$ is the valence of ions, $i$ represents each ion species, $e$ is the elementary charge, $k$ is the Boltzmann constant, and $T = 298$ K is the temperature).

## Viscosity in the orientation chamber

The viscosity is assumed to be constant in the model. However, it is not homogeneous in the orientation chamber, but increases near the glass surface due to the wall effect (35). To analyze the electroorientation with our model, the orientation must be measured at positions sufficiently distant from the glass surface.

To determine the height appropriate for measurement, the viscous coefficient $\eta$ was calculated from the rotational diffusion constant of the microtubules, $D_r$, at various heights above the glass surface (Fig. 1 *C*). The height of each microtubule from the bottom surface of the glass was determined by calibrating the focal plane of the microscope using the fine adjustment knob. The result revealed that the viscosity was constant at a height of 7–22 $\mu$m above the glass surface. Since the focal depth of the microscope was <6 $\mu$m, the electroorientation experiment was conducted on a focal plane 15 $\mu$m above the bottom of the chamber.

## Temperature control

To accurately calculate the viscosity, a constant temperature should be maintained during electroorientation. However, the temperature may increase with the application of the electric field because of excessive Joule heating.

Therefore, we monitored the temperature of the solution using particles of stearic acid butyl ester (S-5001, Sigma) as a temperature indicator. Stearic acid butyl ester is a colorless wax with a melting point of 26.8°C. To monitor the temperature, particles of this wax (10–20 $\mu$m in size) were placed between the electrodes in the LS buffer, and the temperature of the stage was initially set to 24.0 ± 0.2°C. Then, upon application of an alternating electric field of $1.9 \times 10^5$ V/m (1 MHz), the time required to melt the particles was measured. Continuous application of the electric field for a period of 4 s resulted in melting of the particles (i.e., the temperature increased by ~3°C), whereas the repetitive application of the electric field for a period of 3 s with an interval of 7 s left the particles intact.

Based on these results, for the electroorientation conducted at 25.0 ± 0.5°C, we applied an electric field of $<1.9 \times 10^5$ V/m for a period <3 s with an interval >15 s. Under this condition, the increase in temperature of the solution during measurement should be <3°C.

## Calculation of net charge density

The net charges of each $\alpha$- and $\beta$-tubulin subunit at various pH values were calculated by the method of Skoog and Wichman (36), where the number of dissociated charges is obtained by the sum of the charges dissociated from the amino acid side chains and the terminal amino acids. In the calculation, the amino acid sequences of porcine $\alpha$- and $\beta$-tubulin subunits were used (37,38). One molecule each of $Mg^{2+}$ and GTP was included in $\alpha$-tubulin, whereas one molecule of GDP was included in $\beta$-tubulin (39). The net charge of the tubulin dimer was then obtained by summing the net charge of each subunit. The formation of intradimer salt bridges was not taken into consideration in this summation (40) because the dissociated charges that participate in the salt bridge should cancel each other and therefore would not significantly affect the net charge of the dimer. The net charge of the tubulin dimer thus calculated was comparable to the values obtained by molecular dynamics simulation based on the crystal structure of tubulin (41).

# RESULTS AND DISCUSSION

## Observation and quantitative analysis of electroorientation

It has been demonstrated that in response to the applied electric field, parallel arrays of microtubules are formed due to the dipole moment induced along the long axis of the microtubules ((42), K. Sakata, M. Kurachi, and H. Tashiro, RIKEN, personal communication, 1994). We first attempted a reproduction of their results.

When the microtubules in the LS buffer solution (ionic strength 1.11 mM) were initially observed using a dark-field microscope, they exhibited Brownian motion in the chamber, being random in orientation (Fig. 2 *A*, *left*). Upon application of an alternating electric field ($9 \times 10^4$ V/m, 1 MHz), the microtubules were oriented parallel to the field line in a few seconds (Fig. 2 *A*, *right*, and *B*; see Supplementary Material for video). The electroorientation occurred at a field strength $>5 \times 10^4$ V/m and in the frequency range of 10 kHz–5 MHz. At frequencies <10 kHz, the electroorientation was accompanied by a rapid flow of microtubules due to the convection of the solution. This convection can be

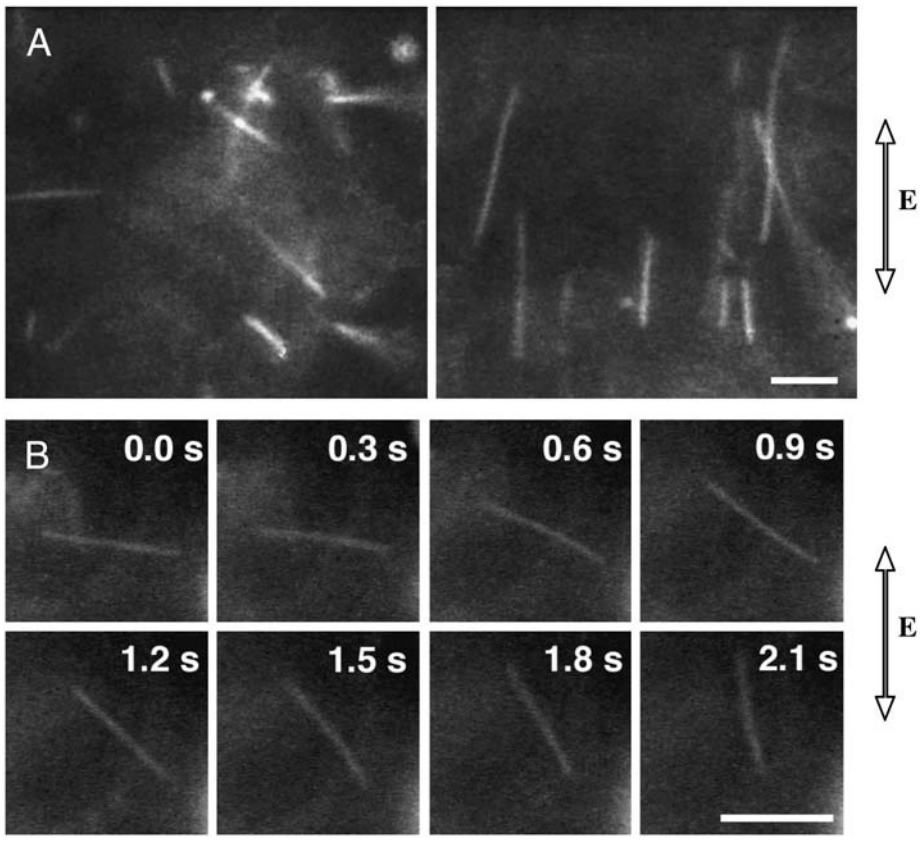


FIGURE 2 Orientation of microtubules at $E = 9 \times 10^4$ V/m, frequency 1 MHz. (*A*, *Left*) Orientation of microtubules is random in the absence of the electric field. (*Right*) Upon application of the electric field, the microtubules are oriented parallel to the direction of the field line. (*B*) Sequential images of a single microtubule after the onset of the electric field taken at intervals of 0.3 s. Arrows indicate the direction of the applied electric field. Scale bar, 10 $\mu$m.

attributed to the ionic current in the solution, as the flow became more obvious when the electroorientation was performed in a solution with higher ionic strength. To avoid convection, a frequency of 1 MHz and a field strength just sufficient to orient the microtubules was used in the following experiments, unless otherwise stated.

The process of electroorientation was analyzed by modeling the microtubule as a dielectric ellipsoid on which electrostatic and viscous countertorques were balanced (see Materials and Methods for details). From the video record of the electroorientation of a single microtubule, the angle of the microtubule long axis against the direction of the field line, $\theta$, was measured frame by frame, and $\ln(\tan\theta)$ was plotted as a function of time (Fig. 3 *A*). As expected from Eq. 8 of the model, $\ln(\tan\theta)$ decreased linearly with time, and the slope gives the inverse of the orientation time constant, $1/\tau$.

When $\tau$ was calculated for microtubules with various lengths, it appeared to be proportional to the square of the microtubule lengths, $l^2$ (Fig. 3 *B*). This result is consistent with the model (Eq. 7), given that the dielectric property of microtubule is homogeneous along its length ($\alpha/l$ = constant). The model also predicts that $\tau$ normalized by $l^2$ should be proportional to $E^{-2}$, where $E$ is the field strength (Eq. 7). This relationship was confirmed with data measured at various field strengths (0.53–1.9 $\times 10^5$ V/m) (Fig. 3 *C*). Together, these results were consistent with the dielectric ellipsoid model; therefore, the effective polarization coefficient of the microtubule, $\alpha$, could be reliably deduced from our measurement. The effective polarization coefficient normalized for the microtubule length, $\alpha/l$, was calculated to be $6.3 \pm 0.3 \times 10^{-24}$ Cm/V at 1 MHz.

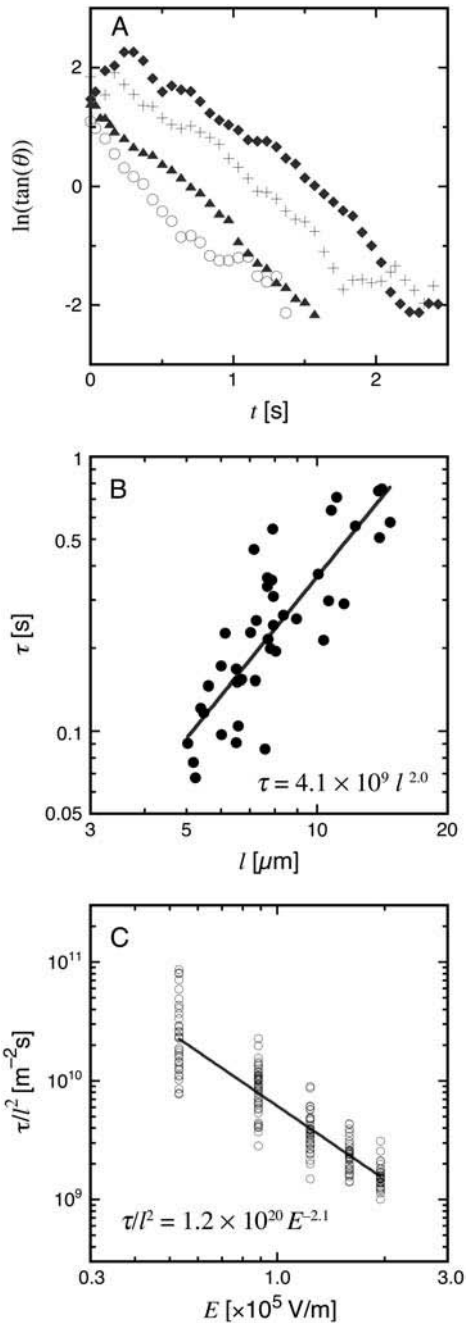


FIGURE 3 Quantitative analysis of microtubule electroorientation. (*A*) $\ln(\tan(\theta))$ plotted against time. Since the taxol-stabilized microtubule is rigid enough, $\theta$ can be uniquely determined at each time instant (see Gittes et al. (56)). Four representative examples for microtubules with lengths of 8–12 $\mu$m are shown. $E = 1.2 \times 10^5$ V/m, frequency 1 MHz. (*B*) Electroorientation time constant $\tau$ plotted as a function of the microtubule length $l$. $\tau$ is proportional to the square of the filament length (line represents the best fit: $\tau = 4.1 \times 10^9\ l^{2.0}$). (*C*) Time constant normalized for the square of microtubule length, $\tau/l^2$, plotted as a function of the field strength $E$. Line represents the best fit: $\tau/l^2 = 1.2 \times 10^{20}\ E^{-2.1}$.

## Dielectric properties of microtubules

The effective polarization coefficient $\alpha = \mathrm{Re}[a_x^* - a_y^*]$ is actually a parameter related to both the conductivity $\sigma_2$ and dielectric constant $\varepsilon_2$ of a microtubule. It is possible to approximate $\sigma_2$ and $\varepsilon_2$ if the frequency dependence of $\alpha$ is known (see Materials and Methods for details).

Fig. 4 *A* shows the spectrum of $\alpha/l$ measured in the frequency range of 10 kHz–7 MHz. Since the dielectric property of the microtubule was homogeneous along its length, the effective polarization constant was normalized by the microtubule length for the purpose of comparison between the frequencies. The magnitude of $\alpha/l$ was almost constant in the frequency range of 30–700 kHz. In the higher frequency range, $\alpha/l$ gradually declined with an increase in the frequency, and the orientation of the microtubule was not observed at frequencies >7 MHz. The gradual decline of $\alpha/l$ is not an artifact due to the voltage drop at high frequencies (see Materials and Methods for details). In contrast, at frequencies <30 kHz, the electroorientation was accompanied by fluid convection, and $\alpha/l$ measured at 10 kHz showed a large deviation.

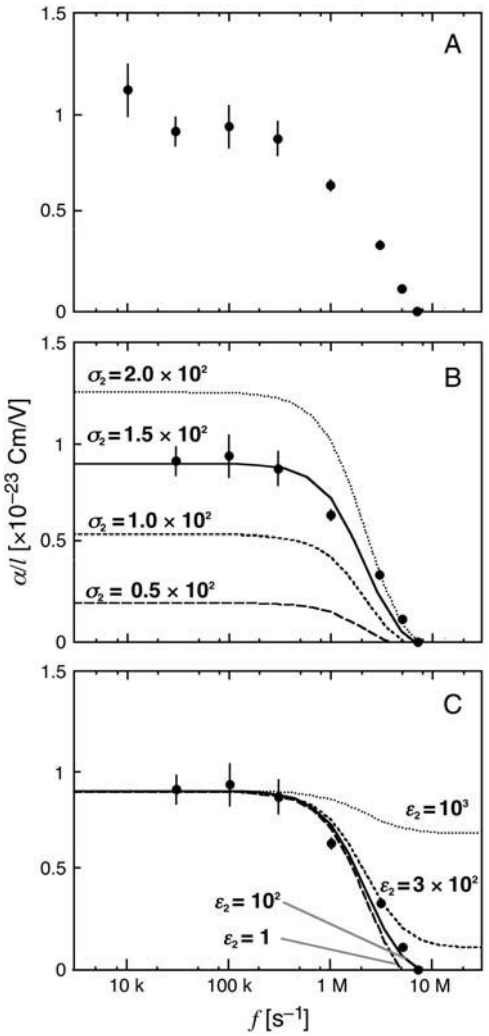


FIGURE 4 Spectrum of the effective polarization coefficient. (*A*) The effective polarization coefficient normalized for the microtubule length, $\alpha/l$, was measured as a function of the frequency of the electric field, $f$. The field strength is just sufficient to orient the microtubules; $E = 0.71$ (<700 kHz), 0.88 (700 kHz), 1.2 (1 MHz), and 1.7 (>1 MHz) $\times$ $10^5$ V/m. Scale bar represents the standard error for 15–20 measurements. (*B*) $\alpha/l$ simulated by Eqs. 3, 9, and 10, assuming $\varepsilon_2 = 10$ and $\sigma_2 = 0.5$, 1.0, 1.5, and 2.0 $\times$ $10^2$ mS/m, respectively. The data obtained at 10 kHz was excluded in this simulation. (*C*) $\alpha/l$ simulated by the same equations, assuming $\sigma_2 = 1.5 \times 10^2$ mS/m and $\varepsilon_2 = 1$, 100, 300, and 1000. In both *B* and *C*, dots represent the measured values.

Fitting the spectrum by Eqs. 3, 9, and 10 using the nonlinear least-squares Marquardt-Levenberg method (with Maxima and GNUPLOT), $\sigma_2$ was estimated to be $1.5 \pm 0.1 \times 10^2$ mS/m (mean $\pm$ SD of the fit) (Fig. 4 *B*). $\varepsilon_2$ was estimated to be <100, but the exact value was not determined. As shown in the simulations, the spectrum is insensitive to the variation of $\varepsilon_2$ when $\varepsilon_2$ is <100 (Fig. 4 *C*).

The microtubule conductivity of $1.5 \times 10^2$ mS/m is ~15 times that of the surrounding medium. Such a high conductivity can be attributed to counterion polarization (22,24,43). A microtubule is a highly negatively charged polymer and is therefore expected to attract counterions from the solution. These counterions are loosely bound to the microtubule, yet they are mobile along its length. In response to the applied electric field, these counterions may move along the long axis of microtubule, resulting in a high microtubule conductivity.

If this interpretation is correct, according to the counterion condensation theory, the conductivity of microtubules should be affected by both their charge density and the counterion species (44,45). To validate this, the following experiments were conducted. Since the spectrum analysis showed that measurement at one frequency is enough to calculate the microtubule conductivity (Fig. 4), the measurements were performed at 1 MHz.

## Effect of ion valence on polarization

The counterion polarization hypothesis predicts that the conductivity of polyelectrolytes might depend on the ion species in the solution. On the other hand, if the electro-orientation is caused by the electronic polarization of the tubulin molecule itself, the conductivity might not depend on the ion species in the solution.

To examine the influence of ion species on the conductivity of microtubules, the electroorientation was examined using various species of monovalent/multivalent ions (Fig. 5). Electroorientation of the microtubules was measured in a solution containing 0.90–1.00 mM MES (pH 6.8), 10 $\mu$M taxol, and 10 $\mu$M of one of the following salts: KCl, NaCl, $ZnCl_2$, $MgCl_2$, $[Co(NH_3)_6]Cl_3$, or $AlCl_3$. Although the microtubules become unstable in the absence of EGTA and $Mg^{2+}$ (46), the filaments remained intact for several hours provided 10 $\mu$M taxol was included in the solution. The result showed that in the presence of monovalent ions such as $K^+$ or $Na^+$, the microtubule conductivity was ~20% higher than that measured with divalent cations. In contrast, in the presence of trivalent cations, the conductivity was ~75% of that measured with divalent cations.

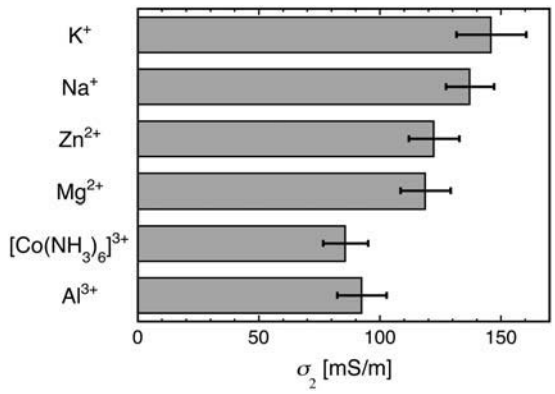


FIGURE 5 Effect of ion species on microtubule conductivity. Conductivity of the solution was adjusted to 9.5 $\pm$ 0.2 mS/m by controlling the concentration of the MES buffer. $E = 1.2 \times 10^5$ V/m. Error bar represents the standard error for 17–26 measurements.

The dependence of microtubule conductivity on ion species might be consistent with the counterion polarization hypothesis. In comparison with cations with lower valences, cations with higher valences are expected to be more strongly bound to the negatively charged surface of the microtubules due to Coulomb interaction (23,24). With an increase in the number of valences, the fraction of counterions being trapped in the so-called Stern layer would increase (34,47), and these trapped counterions should have less mobility compared to the counterions in the diffuse electric double layer (48). Consequently, the conductivity of microtubules in a solution containing ions with higher valences is expected to be lower than that in a solution containing ions with lower valences.

## Effect of charge density on polarization

According to the counterion condensation theory, the formation of counterion clouds depends on the linear charge density of the polyelectrolyte. If the linear charge density of the polyelectrolyte is greater than the critical value ($q_{\text{crit}} = 1/z\lambda_B = 4\pi\varepsilon_0\varepsilon kT/e^2$, where $\varepsilon$ is the relative dielectric constant of the polyelectrolyte, $\varepsilon_0$ is the permittivity of vacuum, $kT$ is the thermal energy, $e$ is the elementary charge, $z$ is the valence of the counterion, and $\lambda_B$ is the so-called ''Bjerrum length''), the counterions will condense around it (24,43). In such a situation, the number of mobile counterions on the polyelectrolyte is expected to be a linear function of its charge density.

To examine the actual relationship between the conductivity and charge density of microtubules, we analyzed the effect of pH on microtubule polarization. By changing the pH of the solution, we varied the degree of dissociation of the charges in tubulin and accordingly modulated the charge density of the microtubules. The result showed that the microtubule conductivity increased as the pH of the solution became farther from the isoelectric point of the microtubules (p$I \approx 4.2$ (49)) (Fig. 6 *A*). We were unable to measure the electroorientation below pH 5.5 because of microtubule depolymerization.

The microtubule conductivities were replotted as a function of the number of net charges per tubulin dimer under each pH condition, which was calculated based on the amino acid composition of tubulin (Fig. 6 *B*). The conductivity appeared to increase linearly with the number of net negative charges, with the $x$-intercept at 20 $e$ per tubulin dimer. This result is consistent with the counterion condensation theory, and the threshold of net negative charges required for electroorientation (20 $e$ per tubulin dimer) may correspond to the critical charge density for counterion condensation.

Baker et al. (12) recently calculated the electrostatic potential for a microtubule structure based on the Poisson-Boltzmann equation. Their result demonstrated that the ribs of a strong negative potential field are formed along the ridges of protofilaments, each intervened by small patches of a positive potential field. This suggests that counterion condensation occurs along the ridges of individual protofilaments rather than occurring homogeneously along the entire surface of the microtubule filament. In keeping with this idea, the threshold of net negative charges derived from our measurement—20 $e$ per tubulin dimer—corresponds to a linear charge density of 2.5 $e$/nm along a protofilament, which is of the same order as the critical charge density theoretically predicted for a linear polyelectrolyte ($q_{\text{crit}} = 1.4$

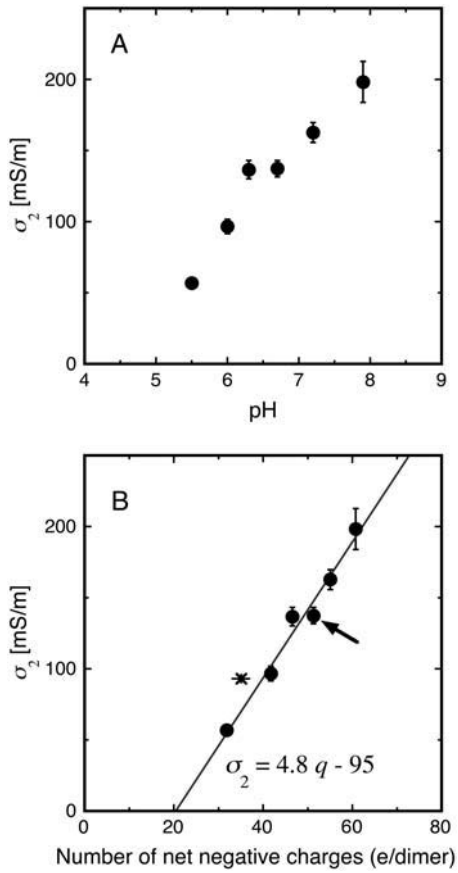


FIGURE 6 Effect of charge density on microtubule conductivity. (*A*) Conductivity of microtubules ($\sigma_2$) measured as a function of pH. Either MES (pH 5–7) or HEPES (pH 7–8) was used to adjust the pH of the medium, whereas the conductivity of the medium was kept constant by controlling the concentration of the buffer solution (9.7 ± 0.3 mS/m). $E = 1.2–1.7 \times 10^5$ V/m. Scale bar represents the standard error for 30–40 measurements. (*B*) Conductivity of microtubules replotted as a function of the number of net charges per tubulin dimer. The arrow indicates the data point measured for intact microtubules at a pH of 6.7, whereas the cross represents the conductivity of the s-MTs measured at the same pH. Since the subtilisin cleavage site was not unique, a range of all plausible charge densities is represented by a horizontal bar (see Materials and Methods for details). The line represents the best fit ($\sigma_2 = 4.8q–95$). It should be noted that our calculation of the net charges (*abscissa*) includes all the dissociated charges in the tubulin dimer and could thus overestimate the surface charges involved in the counterion condensation. Among the dissociated charges included in our calculation, those of some amino acids that are not directly exposed on the microtubule surface may or may not contribute to the counterion condensation.

*e*/nm for monovalent counterions and 0.7 *e*/nm for divalent counterions (see 24,43)).

## Contribution of the C-terminus of tubulin to counterion polarization

In both tubulin $\alpha$- and $\beta$-subunits, negative charges are highly concentrated in the C-terminal region. In each subunit, the disordered C-terminal region of a tubulin emerging from $\alpha-$helix 12, composed of only ~20 amino acid residues (a.a.), contains ~50% of the net negative charges (Table 1) (11). To assess the contribution of this highly acidic region to the conductivity of the microtubule, we examined the electroorientation of s-MTs, in which most of the C-terminal region, <1.5 kDa in size, was deleted from each subunit (50). The result showed that the conductivity of these s-MTs was ~60% that of the intact microtubules; this is consistent with the number of net negative charges expected for s-MTs (Table 2).

It has been observed that the decrease in the number of negative charges in microtubules—whether caused by the protease digestion or a change in the pH—resulted in a reduced microtubule conductivity. As shown in Fig. 6 *B*, the data points fall on the same regression line, represents a linear relationship between the charge density and conductivity of microtubules. These results indicate that all the charges in microtubules equally contribute to the microtubule conductivity.

## Implication of nonspecific electrostatic interactions based on the polyelectrolyte nature of microtubules

Our analyses revealed that the microtubules had a high conductivity, which is probably due to counterion polarization. Counterions are trapped loosely and nonspecifically in the electrostatic field surrounding the microtubules, and they exhibited a behavior typical of counterions in polyelectrolyte solutions. The result was obtained under a low ionic strength condition (~1 mM); therefore, it is not immediately applicable to the physiological ionic condition (>0.1 M).

Nevertheless, under the physiological ionic condition, the fraction of the microtubule surface charges associated with the counterions would be same as that measured under a low ionic strength condition because the number of condensed counterions is determined solely by the charge density of the microtubule. Our result showed a linear relationship between the microtubule conductivity and the charge density with the *x*-intercept at 20 *e* per tubulin dimer (Fig. 6). The result indicates that each protofilament can be approximately considered as a linear polyelectrolyte with the *x*-intercept corresponding to the critical charge density for counterion condensation (24). Thus, based on the counterion condensation theory (23), the fraction of microtubule surface charge compensated by the condensed counterions can be determined by the equation $\theta = 1 - b/z\lambda_B$, where $\lambda_B$ is the Bjerrum length, $z$ is the valence of the counterion, and $b$ is the average charge spacing of the protofilament. At pH 6.8, $b$ is calculated to be 0.15 nm (which is the size of the tubulin dimer, 8 nm, divided by its charge density, 52.2 *e*); hence, $\theta$ is expected to be 79% in a solution of monovalent cations. It may reach 89% in the presence of sufficient divalent cations. The counterion condensation described by this equation is insensitive to the salt concentration in the solution (24,51). In short, at physiological pH and ionic strength, the majority of the microtubule surface charges are expected to be associated with the counterions.

The polyelectrolyte nature of microtubules may underlie the physicochemical mechanism by which microtubules interact with various microtubule-binding proteins. Analogous to the behavior of counterions, some of these binding interactions might be mediated by weak, nonspecific interactions in which the proteins behave simply as polyvalent cations attracted to the negatively charged surface of the microtubules. The interaction does not require the complementary surface of each protein (lock and key mechanism). The stability of the interaction is determined by the charge density of the microtubules and the net positive charges included at the binding site of the proteins. Such nonspecific electrostatic interaction might be involved, for example, in the processive movement of motor proteins such as kinesin and dynein along the microtubule filament (3–5). The weak electrostatic interaction may be advantageous because it may

**TABLE 1 Distribution of charges in tubulin (pH 6.7)**

| | $\alpha$-tubulin | | | $\beta$-tubulin | | |
|---|---|---|---|---|---|---|
| | Intact | w/o C-terminus | C-terminus* | Intact | w/o C-terminus | C-terminus* |
| Number of residues | 451 | 434 | 17 | 445 | 424 | 21 |
| Acidic/basic† | 65/40 | 57/40 | 8/0 | 62/37 | 51/37 | 11/0 |
| Number of net negative charges‡ | 24.8 | 16.7 | 8.1 | 26.1 | 17.2 | 8.9 |
| Relative charge/residue§ | 5.5 | 3.8 | 47.6 | 5.9 | 4.1 | 42.4 |

*C-terminal tail region that has no secondary-structure assignment (54).
†Number of acidic (Asp and Glu) and basic amino acids (Lys and Arg) in the amino acid sequence.
‡The number of net negative charges of intact tubulin, as well as that of tubulin without the C-terminus, was calculated by the method of Skoog and Wichman (36). The number of net charges in the C-terminus was calculated by subtracting the latter from the former value.
§Calculated as 100 × (number of net negative charges/number of residues).

**TABLE 2 Conductivity and net negative charges of intact and subtilisin-treated microtubules at pH 6.7**

| | Intact MT | s-MT* |
|---|---|---|
| Number of residues | 896 | 868–877† |
| Number of net negative charges | 50.9 | 34.2–38.4 |
| $\delta_2 \times 10^2$ mS/m | 1.5 ± 0.07 | 0.96 ± 0.06 |

*Subtilisin-treated microtubules.
†The site of subtilisin digestion was estimated by LC/MS analysis (see Materials and Methods for details).

allow the motors some freedom of motion along the longitudinal axes of microtubules during the weak binding state of the motors.

The stability of the nonspecific protein-microtubule interaction might be affected not only by the electrostatic attraction between the binding pair, but also by the entropy gained by the release of monovalent or divalent cations condensed on the microtubule surface (52,53). As described above, the majority of the microtubule surface charges are associated with counterions; therefore, the binding of cationic proteins would involve the release of counterions into solution, which is accompanied by an entropic gain. Accordingly, the thermal fluctuations of the condensed counterion density along the microtubules may affect/modulate the interaction of cationic proteins with the microtubule.

Regarding protein-protein interaction, we have largely focused on the short-range interaction, which is dependent on the specific, complementary structure of each protein. However, the importance of the weak electrostatic binding interaction, which is probably effective over a long range, has not been recognized until recently (18,34). A better understanding of the latter type of interaction may ultimately lend a new perspective to the function of intermolecular interactions mediated by cytoskeletal filaments. The experiment system developed in this study provides a useful tool to evaluate the polyelectrolyte nature of microtubules. Since the method requires only a small amount of sample ($\sim$1 $\mu$g), it is applicable to isotypically pure microtubules obtained by genetic engineering (Katsuki et al., unpublished). A combination of dielectric measurements and mutational analyses may facilitate future studies aiming to understand the fundamental physicochemical mechanisms underlying the intermolecular interactions of microtubules.

We thank Drs. H. Kondo and H. Tashiro for their help during the microfabrication and the Research Resources Center of RIKEN BSI for the LC/MS analysis. We also thank Drs. M. Suzuki, F. Oosawa, and T. Yamada for their critical comments upon reading this manuscript and Dr. M. Washizu for informative discussions.

## REFERENCES

1. Goldstein, L. S., and Z. Yang. 2000. Microtubule-based transport systems in neurons: the roles of kinesins and dyneins. *Annu. Rev. Neurosci.* 23:39–71.
2. Mandelkow, E., and E. M. Mandelkow. 1995. Microtubules and microtubule-associated proteins. *Curr. Opin. Cell Biol.* 7:72–81.
3. Okada, Y., and N. Hirokawa. 2000. Mechanism of the single-headed processivity: diffusional anchoring between the K-loop of kinesin and the C terminus of tubulin. *Proc. Natl. Acad. Sci. USA.* 97:640–645.
4. Thorn, K. S., J. A. Ubersax, and R. D. Vale. 2000. Engineering the processive run length of the kinesin motor. *J. Cell Biol.* 151:1093–1100.
5. Wang, Z., and M. P. Sheetz. 2000. The C-terminus of tubulin increases cytoplasmic dynein and kinesin processivity. *Biophys. J.* 78:1955–1964.
6. Stebbings, H., and C. Hunt. 1982. The nature of the clear zone around microtubules. *Cell Tissue Res.* 227:609–617.
7. Hirokawa, N. 1994. Microtubule organization and dynamics dependent on microtubule-associated proteins. *Curr. Opin. Cell Biol.* 6:74–81.
8. Scott, C. W., A. B. Klika, M. M. Lo, T. E. Norris, and C. B. Caputo. 1992. Tau protein induces bundling of microtubules in vitro: comparison of different tau isoforms and a tau protein fragment. *J. Neurosci. Res.* 33:19–29.
9. Needleman, D. J., M. A. Ojeda-Lopez, U. Raviv, H. P. Miller, L. Wilson, and C. R. Safinya. 2004. Higher-order assembly of microtubules by counterions: from hexagonal bundles to living necklaces. *Proc. Natl. Acad. Sci. USA.* 101:16099–16103.
10. Tokuraku, K., K. Matsushima, T. Matui, H. Nakagawa, M. Katsuki, R. Majima, and S. Kotani. 2003. The number of repeat sequences in microtubule-associated protein 4 affects the microtubule surface properties. *J. Biol. Chem.* 278:29609–29618.
11. Tuszynski, J. A., J. A. Brown, E. Crawford, E. J. Carpenter, M. L. A. Nip, J. M. Dixon, and M. V. Sataric. 2005. Molecular dynamics simulations of tubulin structure and calculations of electrostatic properties of microtubules. *Math. Comput. Model.* 41:1055–1070.
12. Baker, N. A., D. Sept, S. Joseph, M. J. Holst, and J. A. McCammon. 2001. Electrostatics of nanosystems: application to microtubules and the ribosome. *Proc. Natl. Acad. Sci. USA.* 98:10037–10041.
13. Takashima, S. 1989. Electrical Properties of Biopolymers and Membranes. Adam Hilger, Bristol and Philadelphia.
14. Bloomfield, V. A. 1991. Condensation of DNA by multivalent cations: considerations on mechanism. *Biopolymers.* 31:1471–1481.
15. Tang, J. X., and P. A. Janmey. 1996. The polyelectrolyte nature of F-actin and the mechanism of actin bundle formation. *J. Biol. Chem.* 271:8556–8563.
16. Tang, J. X., T. Ito, T. Tao, P. Traub, and P. A. Janmey. 1997. Opposite effects of electrostatics and steric exclusion on bundle formation by F-actin and other filamentous polyelectrolytes. *Biochemistry.* 36: 12600–12607.
17. Gelbart, W. M., R. F. Bruinsma, P. A. Pincus, and V. A. Parsegian. 2000. DNA-inspired electrostatics. *Phys. Today.* 53:38–44.
18. Levin, Y. 2002. Electrostatic correlations: from plasma to biology. *Rep. Prog. Phys.* 65:1577–1632.
19. Angelini, T. E., H. Liang, W. Wriggers, and G. C. Wong. 2003. Like-charge attraction between polyelectrolytes induced by counterion charge density waves. *Proc. Natl. Acad. Sci. USA.* 100:8634–8637.
20. Jones, T. B. 1995. Electromechanics of Particles. Cambridge University Press, Cambridge.
21. Goater, A. D., and R. Pethig. 1998. Electrorotation and dielectrophoresis. *Parasitology.* 117(Suppl.):S177–S189.
22. Mandel, M. 1961. The electric polarization of rod-like, charged macromolecules. *Mol. Phys.* 4:489–496.
23. Manning, G. S. 1978. The molecular theory of polyelectrolyte solutions with applications to the electrostatic properties of polynucleotides. *Q. Rev. Biophys.* 11:179–246.
24. Oosawa, F. 1971. Polyelectrolytes. Marcel Dekker, New York.
25. Shelanski, M. L., F. Gaskin, and C. R. Cantor. 1973. Microtubule assembly in the absence of added nucleotides. *Proc. Natl. Acad. Sci. USA.* 70:765–768.

26. Himes, R. H., P. R. Burton, and J. M. Gaito. 1977. Dimethyl sulfoxide-induced self-assembly of tubulin lacking associated proteins. *J. Biol. Chem.* 252:6222–6228.

27. Kristofferson, D., T. Mitchison, and M. Kirschner. 1986. Direct observation of steady-state microtubule dynamics. *J. Cell Biol.* 102:1007–1019.

28. Serrano, L., J. Avila, and R. B. Maccioni. 1984. Controlled proteolysis of tubulin by subtilisin: localization of the site for MAP2 interaction. *Biochemistry.* 23:4675–4681.

29. Goldstein, D. A. 1979. Calculation of the concentrations of free cations and cation-ligand complexes in solutions containing multiple divalent cations and ligands. *Biophys. J.* 26:235–242.

30. Schwan, H. P. 1963. Determination of biological impedances. *In* Physical Techniques in Biological Research, Vol. 6. G. Oster, editor. Academic Press, New York. 323–407.

31. Miller, R. D., and T. B. Jones. 1987. Frequency-dependent orientation of ellipsoidal particles in AC electric fields. *Proc. IEEE 9th Annu. EMBS Conf. Boston.*:710–711.

32. Washizu, M., M. Shikida, S. Aizawa, and H. Hotani. 1992. Orientation and transformation of flagella in electrostatic field. *IEEE Trans. Ind. Appl.* 28:1194–1202.

33. Miller, R. D., and T. B. Jones. 1993. Electro-orientation of ellipsoidal erythrocytes. Theory and experiment. *Biophys. J.* 64:1588–1595.

34. Israelachvili, J. N. 1992. Intermolecular and Surface Forces. Academic Press, San Diego.

35. Happel, J., and H. Brenner. 1973. Low Reynolds Number Hydrodynamics. Martinus Nijhoff, The Hague.

36. Skoog, B., and A. Wichman. 1986. Calculation of the isoelectric points of polypeptides from the amino acid composition. *Trends Anal. Chem.* 5:82–83.

37. Ponstingl, H., E. Krauhs, M. Little, and T. Kempf. 1981. Complete amino acid sequence of alpha-tubulin from porcine brain. *Proc. Natl. Acad. Sci. USA.* 78:2757–2761.

38. Krauhs, E., M. Little, T. Kempf, R. Hofer-Warbinek, W. Ade, and H. Ponstingl. 1981. Complete amino acid sequence of beta-tubulin from porcine brain. *Proc. Natl. Acad. Sci. USA.* 78:4156–4160.

39. Menendez, M., G. Rivas, J. F. Diaz, and J. M. Andreu. 1998. Control of the structural stability of the tubulin dimer by one high affinity bound magnesium ion at nucleotide N-site. *J. Biol. Chem.* 273:167–176.

40. Nogales, E., M. Whittaker, R. A. Milligan, and K. H. Downing. 1999. High-resolution model of the microtubule. *Cell.* 96:79–88.

41. Tuszynski, J. A., T. Luchko, E. J. Carpenter, and E. Crawford. 2004. Results of molecular dynamics computations of the structural and electrostatic properties of tubulin and their consequences for microtubules. *J. Comput. Theor. Nanosci.* 1:392–397.

42. Vassilev, P. M., R. T. Dronzine, M. P. Vassileva, and G. A. Georgiev. 1982. Parallel arrays of microtubules formed in electric and magnetic fields. *Biosci. Rep.* 2:1025–1029.

43. Manning, G. S. 1972. Polyelectrolytes. *Annu. Rev. Phys. Chem.* 23: 117–140.

44. Takashima, S. 1967. Effect of ions on the dielectric relaxation of DNA. *Biopolymers.* 5:899–913.

45. Fornés, J. A. 2000. Dielectric relaxation around a charged colloidal cylinder in an electrolyte. *J. Colloid Interface Sci.* 222:97–102.

46. Olmsted, J. B., and G. G. Borisy. 1975. Ionic and nucleotide requirements for microtubule polymerization in vitro. *Biochemistry.* 14:2996–3005.

47. Besteman, K., M. A. Zevenbergen, H. A. Heering, and S. G. Lemay. 2004. Direct observation of charge inversion by multivalent ions as a universal electrostatic phenomenon. *Phys. Rev. Lett.* 93:170802.

48. Joly, L., C. Ybert, E. Trizac, and L. Bocquet. 2004. Hydrodynamics within the electric double layer on slipping surfaces. *Phys. Rev. Lett.* 93:257805.

49. Stracke, R., K. J. Bohm, L. Wollweber, J. A. Tuszynski, and E. Unger. 2002. Analysis of the migration behaviour of single microtubules in electric fields. *Biochem. Biophys. Res. Commun.* 293:602–609.

50. Sackett, D. L., and J. Wolff. 1986. Proteolysis of tubulin and the substructure of the tubulin dimer. *J. Biol. Chem.* 261:9070–9076.

51. Manning, G. S. 1969. Limiting laws and counterion condensation in polyelectrolyte solutions. I. Colligative Properties. *J. Chem. Phys.* 51: 924–933.

52. Anderson, C. F., and M. T. Record, Jr. 1995. Salt-nucleic acid interactions. *Annu. Rev. Phys. Chem.* 46:657–700.

53. Anderson, C. F., and M. T. Record, Jr. 1990. Ion distributions around DNA and other cylindrical polyions: theoretical descriptions and physical implications. *Annu. Rev. Biophys. Biophys. Chem.* 19:423–465.

54. Nogales, E., S. G. Wolf, and K. H. Downing. 1998. Structure of the alpha beta tubulin dimer by electron crystallography. *Nature.* 391:199–203.

55. Berg, H. 1993. Random Walks in Biology. 2nd ed. Princeton University Press, Princeton.

56. Gittes, F., B. Mickey, J. Nettleton, and J. Howard. 1993. Flexural rigidity of microtubules and actin filaments measured from thermal fluctuations in shape. *J. Cell Biol.* 120:923–934.